

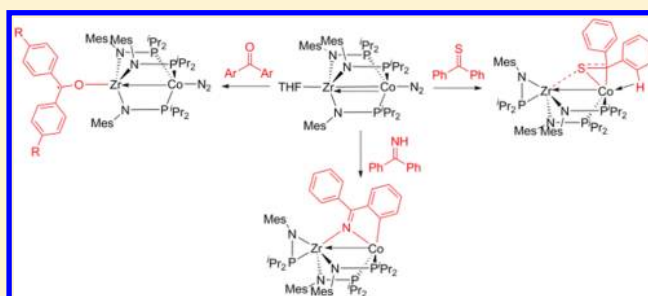
Interaction and Activation of Carbon–Heteroatom π Bonds with a Zr/Co Heterobimetallic Complex

Seth L. Marquard, Mark W. Bezpalko, Bruce M. Foxman, and Christine M. Thomas*

Department of Chemistry, Brandeis University, 415 South Street, Waltham, Massachusetts 02454, United States

S Supporting Information

ABSTRACT: Single-electron transfer from the $\text{Zr}^{\text{IV}}\text{Co}^{-\text{I}}$ heterobimetallic complex $(\text{THF})\text{Zr}(\text{MesNP}^i\text{Pr}_2)_3\text{Co}-\text{N}_2$ (**1**) to benzophenone was previously shown to result in the isobenzopinacol product $[(\text{Ph}_2\text{CO})\text{Zr}(\text{MesNP}^i\text{Pr}_2)_3\text{Co}-\text{N}_2]_2$ (**4**) via coupling of two ketyl radicals. Thermolysis of **4** led to cleavage of the $\text{C}=\text{O}$ bond to generate a Zr/Co μ -oxo species featuring an unusual terminal $\text{Co}=\text{CPh}_2$ carbene linkage (**3**). In this work monomeric ketyl radical complexes have been synthesized, and the reactivity of these compounds has been explored. The electronic preference for the formation of a ketyl radical complex or a coordination complex has been investigated computationally. Furthermore, thione substrates were allowed to react with **1**, generating new complexes that bind the thione to the Co rather than undergoing single-electron transfer (**12**, **14**). The preference of thiones to coordinate to Co can be overridden if the Co is ligated by CO, in which case a thioketyl radical complex forms (**13**) analogous to **4**. The reaction between **1** and imines resulted in N–H bond activation, affording a μ -methyleneamido Co–H complex (**16**) that can undergo cyclometalation and loss of H_2 (**15**).



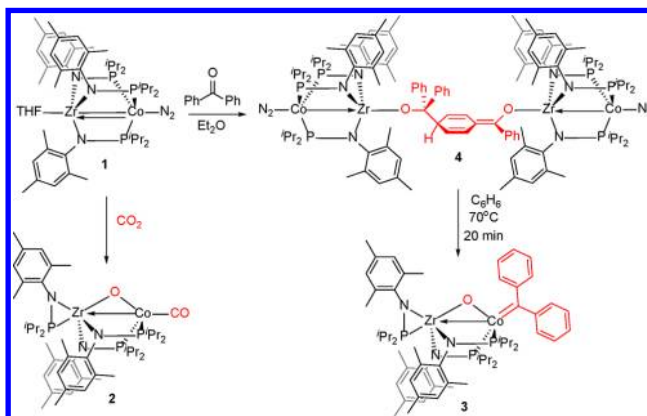
INTRODUCTION

Understanding and predicting the activation of strong σ and π bonds by transition-metal complexes remains a formidable synthetic challenge. Activation of C–H, N–H, O–H, and other σ bonds has been explored as fundamental steps in cross-coupling reactions as well as alkane and alkene functionalizations.^{1–4} The activation of C=C, C=N, C=O, and C=S bonds could expand the understanding of bond cleavage reactions and expand the scope of synthetic methods to utilize these functional groups. Deoxygenation of CO to a surface-bound methylene is a proposed step in the Fischer–Tropsch synthesis of hydrocarbons, but the mechanism of this heterogeneous reaction is not well understood.⁵ Homogeneous deoxygenation of ketones has been demonstrated by Ti(III) complexes,⁶ tungsten complexes,^{7,8} and a Zr–Fe heterobimetallic species.⁹ Desulfurization of C=S bonds is less well-known, but a few examples with early and late transition metals are known. For example, early transition metals such as titanium(III) desulfurize thiobenzophenone to afford tetraphenylethylene,⁶ and the oxidative addition of the C=S bond across a Mo–Mo or W–W homobimetallic complex has been reported.¹⁰ The late transition metals ruthenium and iron have also been shown to react with C=S bonds. Tobita reported a silylene ruthenium complex that reacts with isothiocyanates resulting in C=S bond cleavage,¹¹ and desulfurization of *N,N*-dimethylthioformamide to afford an iron carbene was reported by Nakazawa.¹²

Over the past several years our group has focused on the functionalization and activation of small molecules by the

highly reduced heterobimetallic complex $(\text{THF})\text{Zr}(\text{MesNP}^i\text{Pr}_2)_3\text{Co}-\text{N}_2$ (**1**).^{13–15} We demonstrated that the $\text{C}=\text{O}$ bond of carbon dioxide is cleaved, affording the μ -oxo/Co-carbonyl complex **2**,¹³ and recently we have shown that ketones undergo a similar transformation, yielding the μ -oxo/Co-carbene complex **3** (Scheme 1).¹⁶ The rapid reaction of **1** with CO_2 to cleave a $\text{C}=\text{O}$ bond is of obvious importance in the context of sustainable strategies for utilizing CO_2 as a useful C_1 feedstock. However, the mechanism by which this

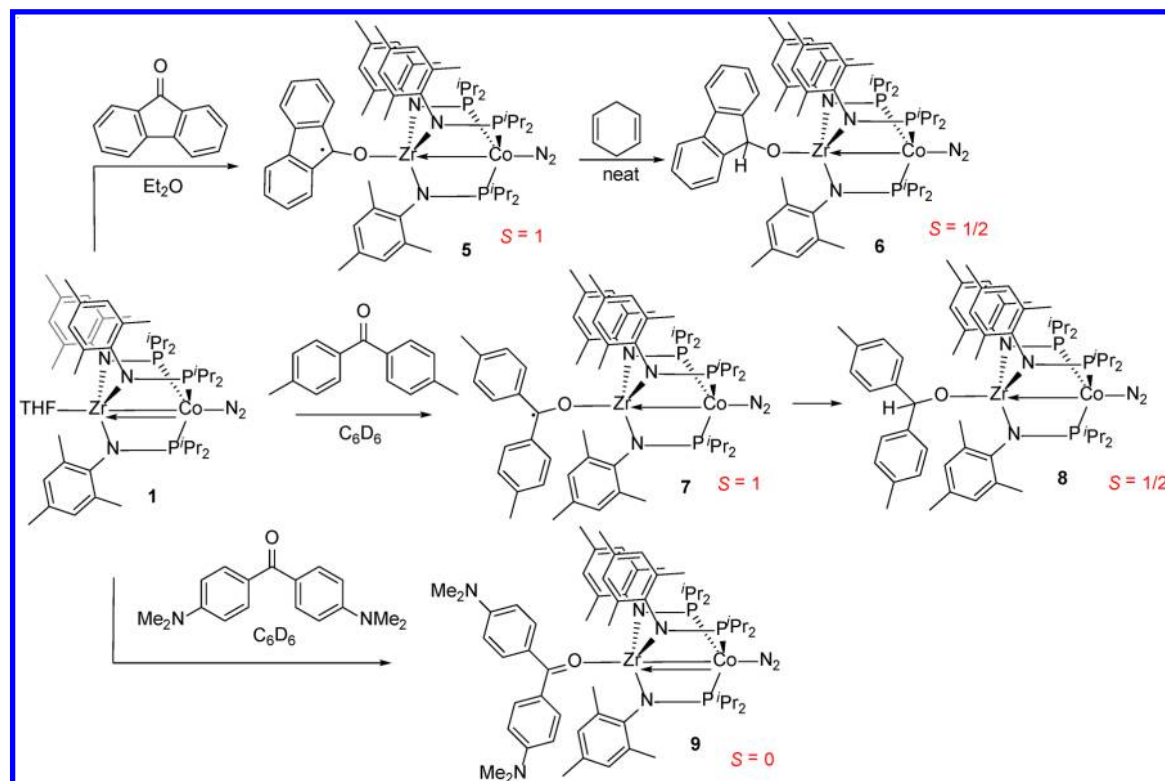
Scheme 1



Received: March 2, 2014

Published: April 9, 2014

Scheme 2



reaction occurs is not well understood and could involve either a concerted two-electron pathway or a stepwise single-electron-transfer mechanism. The activation of C=O bonds in ketones may serve as a useful model to understand the activation of CO₂ and may also lead to new manifolds for synthetic chemistry. In an effort to further explore the activation of carbon–heteroatom double bonds by our Zr/Co complex, we have turned our attention to the reaction of **1** with substrates containing C=E (E = O, N, S) bonds to interrogate the effect of the heteroatom and its substituents on the bond activation products.

RESULTS AND DISCUSSION

Reactivity of 1 with Ketones. We previously reported that the stoichiometric addition of benzophenone to **1** afforded the isobenzopinacol-bridged tetrametallic complex **4** arising through radical coupling (Scheme 1).¹⁷ Similar reactions had been previously reported and well-studied with well-defined Ti^{III} complexes.^{18,19} Under thermal conditions, **4** is proposed to dissociate into a monomeric ketyl radical complex before the formation of a μ -oxo/Co-carbene complex (**3**). We sought to prepare and isolate a monomeric ketyl radical complex to validate this hypothesis and to investigate the chemistry of such Zr-bound ketyl radical intermediates. We were pleased to find that a monomeric ketyl radical compound could be isolated by the reaction of complex **1** with fluorenone, affording complex **5** as a dark red crystalline solid (Scheme 2). The ¹H NMR spectrum of complex **5** was broad and exhibited eight paramagnetically shifted peaks, suggesting a reasonably symmetric complex that had not dimerized in a fashion similar to **4**. Consistent with a triplet ground state, the solution magnetic moment of complex **5** measured using the Evans' method is 2.5 μ_B . The stretching frequency of the N₂ ligand in

complex **5** is 2059 cm⁻¹, which is higher than that in **4** (2046 cm⁻¹), indicative of an oxidized Co center.

X-ray crystallographic analysis of single crystals of **5** revealed the monomeric pseudo-C₃-symmetric structure, shown in Figure 1. The Zr–O (2.0169(11) Å) and C–O (1.3265(19)

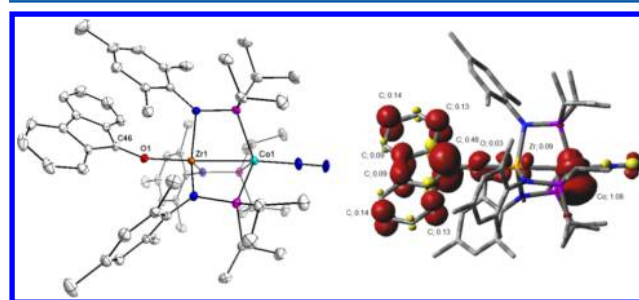


Figure 1. (left) Displacement ellipsoid (50%) representation of complex **5**. Hydrogen atoms have been omitted for clarity. Selected interatomic distances (Å): Zr1–Co1, 2.6324(3); Zr1–O1, 2.0169(11); O1–C46, 1.3265(19). (right) Computed unpaired spin density surface of complex **5**.

Å) bond distances of **5** are analogous to those in the Zr fluorenone ketyl radical complex Cp*₂ZrCl(fluorenone) reported by Hou and co-workers (Zr–O = 2.00 Å and C–O = 1.32 Å).²⁰ The Zr–Co interatomic distance in **5** is 2.6324(3) Å in comparison to 2.36 Å in **1**, suggesting a much weaker metal–metal interaction upon one-electron oxidation of the Zr/Co unit. A computational analysis of the electronic structure of complex **5** at the BP86/LANL2TZ(f)/6-311+G(d)/D95 V level of theory reveals that one unpaired electron is distributed on the Co center (1.07e) and one unpaired electron is delocalized throughout the aromatic π system of the

fluorenone, with a small amount of spin on Zr (0.09e). A plot of the spin density is shown in Figure 1.

Although the isobenzopinacol-bridged tetrametallic complex undergoes thermal C=O cleavage to afford a Co carbene,¹⁶ complex **5** does not undergo the same transformation. This key difference could be a result of the fused-ring system present in fluorenone but absent in benzophenone. We have noted other fundamental differences in the reactivity of other benzophenone and fluorenone derivatives (*vide infra*). We had previously suggested that a ketyl radical intermediate such as **5** was on the reaction pathway for catalytic hydrosilylation of ketones and that C–H bond formation proceeded via abstraction of an H atom from the PhSiH₃ reductant.¹⁷ Consistent with this hypothesis, a considerable kinetic isotope effect ($k_{\text{H}}/k_{\text{D}} = 2.4$) was observed. To further support that H atom abstraction was possible for a ketyl radical, complex **5** was allowed to react with 1,4-cyclohexadiene at room temperature, resulting in hydrogen atom abstraction to afford the yellow alkoxide complex **6** (Scheme 2). In contrast, the reaction of isobenzopinacol complex **4** with 1,4-cyclohexadiene does not occur at room temperature and at elevated temperatures proceeds to carbene complex **3** rather than the alkoxide.

The ¹H NMR spectrum of **6** shows nine broad paramagnetically shifted resonances, consistent with a pseudo-3-fold symmetric structure. The newly formed C–H bond in the alkoxide is clearly visible as a singlet at 9.94 ppm in the ¹H NMR spectrum. Evans' method data collected on a solution of **6** reveal a decreased magnetic moment, consistent with a single unpaired electron remaining on the Co⁰ center. The stretching frequency of the N₂ ligand present in **6** is 2044 cm⁻¹, which is consistent with those for other alkoxide complexes.²¹ X-ray diffraction was carried out on single crystals of complex **6**, revealing the solid-state structure shown in Figure 2.

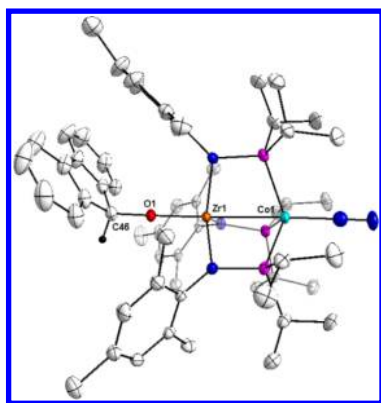


Figure 2. Displacement ellipsoid representation (50%) of complex **6**. Hydrogen atoms and a cocrystallized 2,4,6-trimethylaniline molecule have been omitted for clarity. A disordered *p*-Me group of one of the mesityl rings was adequately modeled, and for clarity only one of two possible positions is shown (see the Supporting Information for more crystallographic details). Selected interatomic distances (Å): Zr1–Co1, 2.6958(5); Zr1–O1, 1.9446(18); O1–C46, 1.420(3).

Comparison of the Zr–O and C–O bond distances in the solid-state structures of **5** and **6** reveals a contraction of the Zr–O bond (2.0169(11) Å in **5**; 1.9446(18) Å in **6**) and an increase in the C–O bond (1.3265(19) Å in **5**; 1.420(3) Å in **6**), consistent with the formation of an alkoxide with a C–O single bond and a more covalent Zr–O interaction. As the Zr–O interaction becomes stronger, the Zr–Co interaction trans to

it becomes weaker, as evidenced by an elongation of the Zr–Co distance in complex **6** (2.6958(5) Å) in comparison to complex **5** (2.6324(3) Å).

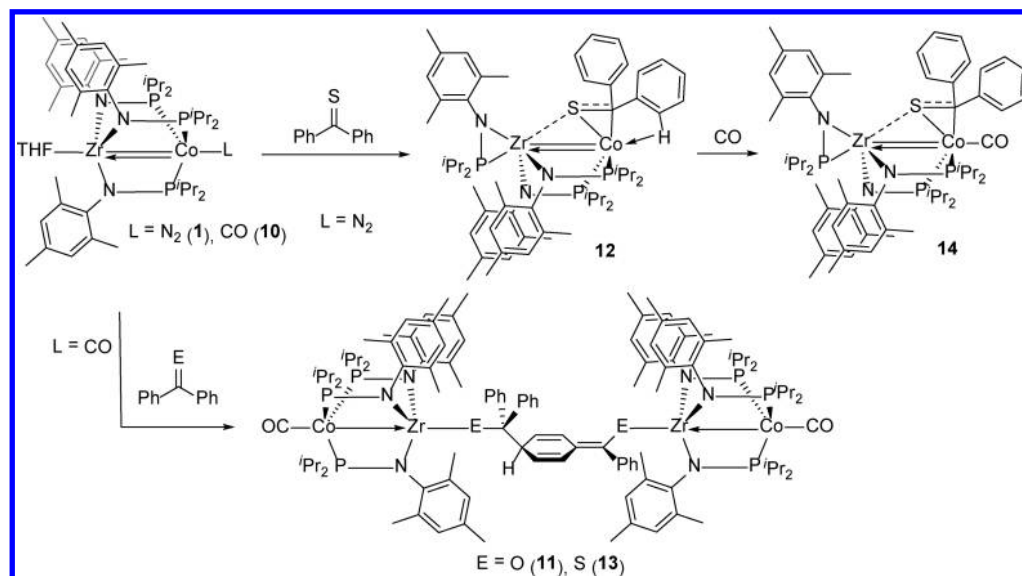
On the basis of the fundamental differences in the reactivity between fluorenone and benzophenone, we began to explore the reaction between **1** and several other benzophenone derivatives with para substituents in place to prevent radical coupling. Allowing **1** to react with 4,4'-dimethylbenzophenone immediately afforded a dark red solution of the paramagnetic ($S = 1$) monomeric ketyl radical complex **7**. Complex **7** is only transiently stable, and ¹H NMR spectra of samples of **7** were consistently contaminated with the alkoxide **8** ($S = 1/2$). Complex **8** is formed from **7** by hydrogen atom abstraction from the stoichiometric quantity of THF present from complex **1** (Scheme 2),²² and due to this facile process, we were unable to isolate complex **7** even at low temperature (–35 °C).

In contrast to the ketone substrates explored above, the reaction between **1** and bis(4,4'-dimethylamino)benzophenone afforded the diamagnetic ketone adduct **9** (Scheme 2). Complex **9** was characterized by ¹H, ³¹P{¹H}, and ¹³C{¹H} NMR experiments, which revealed the replacement of the THF ligand present in **1** with the diaryl ketone. The IR spectrum of complex **9** has a diagnostic N₂ stretch at 2044 cm⁻¹, confirming that N₂ remains bound to cobalt, as well as a stretch for the bound ketone at 1601 cm⁻¹, implying that the carbon–oxygen double bond remains intact. While we were unable to obtain X-ray-quality crystals of **9**, the geometry derived computationally (*vide infra*) features a Zr–Co distance (2.53 Å) much shorter than those in the $S = 1$ complexes discussed previously. Thermolysis of **9** did not afford a carbene complex analogous to **3**, suggesting that formation of a ketyl radical is a prerequisite for the C=O bond cleavage reaction.

From the above results, it is evident that electronic parameters of the substrate play an important role in dictating the formation of an $S = 1$ ketyl radical complex or a simple $S = 0$ ketone adduct. Evidence for the formation of a Zr–ketone adduct in the absence of electron transfer (complex **9**) suggests that initial coordination of the ketone to Zr is a key step. The carbonyl analogue of **1**, (THF)Zr(MesNP^{*i*}Pr₂)₃Co–CO (**10**), in which the CO ligand has been found to be far less labile than N₂,²³ was used to probe this hypothesis. Allowing benzophenone to react with the reduced carbonyl complex **10** afforded a new paramagnetic yellow complex (**11**) with a ¹H NMR spectrum similar to that of the isobenzopinacol coupling product **4** (Scheme 3). The stretching frequency of the CO ligand is 1889 cm⁻¹ for complex **11**, which is in the range of those for previously reported (alkoxide)Zr(MesNP^{*i*}Pr₂)₃Co–CO complexes.²³ This result demonstrates that initial coordination of the substrate occurs at the Zr side of the molecule. Subsequent electron transfer would then proceed through the metal–metal interaction to the Zr-bound ketone. In cases where the diaryl ketone is electron-rich, such as bis(4,4'-dimethylamino)benzophenone, electron transfer is disfavored, leading to a diamagnetic ketone adduct (**9**).

To further investigate the substituent effects on single-electron transfer to ketones, a series of (Ar₂CO)Zr(MesNP^{*i*}Pr₂)₃CoN₂ complexes were computationally investigated to determine the differences in energy between the singlet ketone adduct (Ar₂C=O)Zr^{IV}(MesNP^{*i*}Pr₂)₃Co⁻¹N₂ and the triplet ketyl radical (Ar₂C[•]O)Zr^{IV}(MesNP^{*i*}Pr₂)₃Co⁰N₂. Consistent with our experimental observations, the triplet states of the benzophenone and dimethylbenzophenone derivatives were calculated to be 3.9 and 2.7 kcal/mol lower in energy than

Scheme 3



the singlet, respectively. The singlet state of the dimethylamino-substituted derivative, however, was predicted to be favored over the triplet by 2.8 kcal/mol, in good agreement with our experimental observations. Several other derivatives were calculated *in silico* to explore the trend, revealing that a triplet state is preferred by 7.0 kcal/mol with *p*-CONH₂ substituents and the singlet ketone adduct is very slightly favored by 0.6 kcal/mol for the *p*-NH₂ derivative. A plot of the difference in energy between the *S* = 0 ketone adduct and the *S* = 1 ketyl radical complex as a function of the Hammett parameter of the ketone para substituent (σ_p)²⁴ reveals a linear correlation (Figure 3).

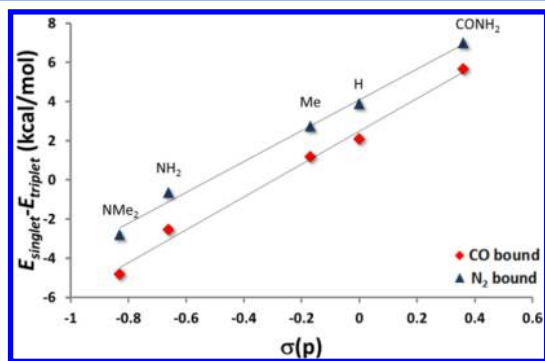


Figure 3. Plot of the calculated difference in energy between the singlet ketone adduct ((*p*-XAr)₂C=O)Zr^{IV}(MesNPⁱPr₂)₃Co⁻¹-L and the triplet ketyl radical complex (((*p*-XAr)₂C[•]-O)-Zr^{IV}(MesNPⁱPr₂)₃Co⁰-L vs the Hammett parameter (σ_p)²⁴ of the para substituent (X), where L = CO ($R^2 = 0.99$), N₂ ($R^2 = 0.99$). See the Experimental Section and Supporting Information for computational details.

A similar linear correlation between the energetic preferences for the singlet vs triplet state was observed for the hypothetical Co carbonyl complexes (Ar₂CO)Zr(MesNPⁱPr₂)₃Co-CO (Figure 3). In contrast to the N₂-bound complexes, a stronger preference for the singlet state is observed when the stronger π acceptor CO is bound to cobalt, resulting in a trend line with a similar slope but a decreased *y* intercept. For example, once CO is bound, the ketyl radical state of the parent benzophenone

derivative is now only favored by 2.1 kcal/mol, and the singlet ketone adduct is favored for the *p*-NMe₂ derivative by 4.8 kcal/mol.

The singlet/triplet preference can easily be explained by trends in the one-electron-reduction potential of benzophenone derivatives as a function of para substituent. Single-electron transfer occurs to generate the triplet ketyl radical complex when the reduction potential of the ketone is more positive, while electron transfer does not occur when the ketone is more electron rich and more difficult to reduce ($E_{1/2}$ of benzophenone, -1.84 V; $E_{1/2}$ of *p*-NMe₂-benzophenone, -2.16 V). A plot of the difference in energy between the *S* = 0 and *S* = 1 states vs the diaryl ketone redox potential also reveals a linear correlation (Figure 4).²⁵

Reactivity of 1 with Thiones. From the differences noted between simple ketone derivatives, we decided to investigate the effect the heteroatom has on the C=Y activation reaction. Treatment of 1 with thiobenzophenone afforded the purple diamagnetic complex 12 (Scheme 3). The ¹H NMR spectrum of 12 reveals an asymmetric product with inequivalent

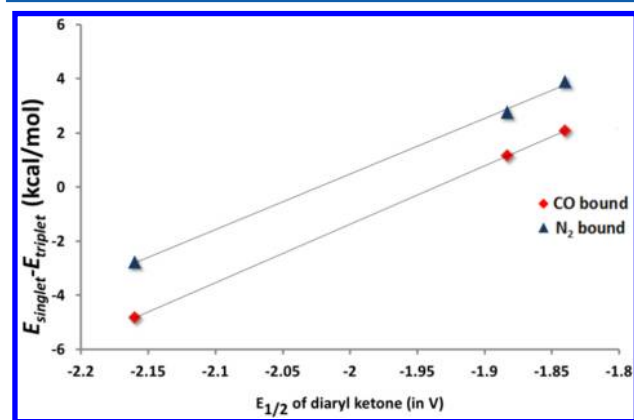


Figure 4. Plot of the calculated difference in energy between the singlet ketone adduct ((*p*-XAr)₂C=O)Zr^{IV}(MesNPⁱPr₂)₃Co⁻¹-L and the triplet ketyl radical complex (((*p*-XAr)₂C[•]-O)-Zr^{IV}(MesNPⁱPr₂)₃Co⁰-L vs the $E_{1/2}$ value of the diaryl ketone,²⁵ where L = CO ($R^2 = 1.00$), N₂ ($R^2 = 0.99$).

phosphinoamide ligands. The $^{31}\text{P}\{^1\text{H}\}$ NMR spectrum of **12** reveals two signals at 49.54 and 15.90 ppm, corresponding to two ligands bridging the Zr and Co centers, and one ligand dissociated from Co and η^2 -bound to the Zr center.

To elucidate the structure of **12**, single crystals suitable for X-ray diffraction were grown. The solid-state structure shown in Figure 5 was obtained, confirming an asymmetric structure with

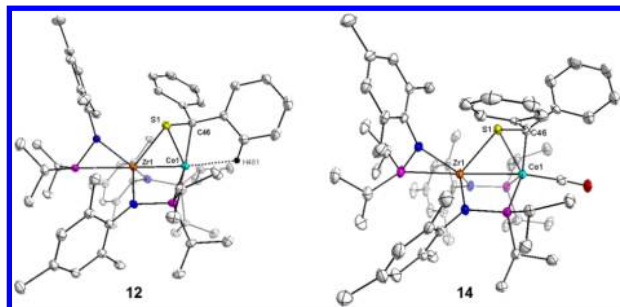


Figure 5. Displacement ellipsoid (50%) representation of complexes **12** and **14**. Hydrogen atoms, except for H481 and an ether solvate molecule in the asymmetric unit of **12**, have been omitted for clarity. Selected interatomic distances (Å) for **12**: Zr1–Co1, 2.3857(2); Zr1–S1, 2.6866(4); Co1–S1, 2.2062(4); Co1–C46, 2.0203(14); C46–S1, 1.8073(15); Co1–H481, 2.32. Selected interatomic distances (Å) for **14**: Zr1–Co1, 2.7072(5); Zr1–S1, 2.5677(9); Co1–S1, 2.2252(9); Co1–C46, 2.099(3); C46–S1, 1.787(3).

an η^2 -phosphinoamide ligand. Rather than binding to the Zr center, the thione binds η^2 to Co through the C=S π bond, with the S atom in a position bridging the Zr and Co centers. The C–S bond is elongated (1.8073(15) Å) in comparison to that in free thiobenzophenone (1.636(9) Å)²⁶ and is within the range of C–S distances found in Ni, Pt, and V thiobenzophenone π complexes reported in the literature (1.76–1.81 Å).^{27–30} The geometry about the thioketone carbon C46 is pyramidalized, with an angle of 137° between the C–S bond vector and the C–C46–C plane. The Zr–S distance (2.6866(4) Å) is much longer than the Co–S distance (2.2062(4) Å), suggesting stronger binding to Co, as would be expected on the basis of hard/soft acid base predictions. In addition to binding to Co through the C and S atoms, the solid-state structure reveals a weak agostic interaction between Co and one of the ortho hydrogen atoms of the thione (Co–H481 = 2.32 Å). The Zr–Co distance in complex **12** remains quite short (2.3867(2) Å), implying that a substantial Co→Zr interaction remains despite coordination and partial activation of the C=S bond.

The isolation of complex **12** rather than a thioketyl radical complex was unexpected, because the one-electron reduction potential of thiobenzophenone is ~0.7 V more positive than that of benzophenone ($E_{1/2}$ of thiobenzophenone, –1.17 V; $E_{1/2}$ of benzophenone, –1.84 V).²⁵ However, the preference of thiobenzophenone to bind to Co may dictate the different reactivity observed. The decreased nucleophilicity of sulfur in thiobenzophenone is also a well-known phenomenon in the organometallic chemistry of thiobenzophenone. Addition of nucleophiles such as alkylolithiums and Grignard reagents proceeds via nucleophilic attack at sulfur rather than the carbon in thioketone derivatives.^{31,32} Such polarization of the C=S bond would disfavor binding of sulfur to the Lewis acidic Zr center, favoring addition to the more electron rich Co center of **1** instead. Furthermore, the radical anions of thioketones have been shown to have significant spin delocalization on the

sulfur atom, which may contribute to the preference for the formation of **12**, rather than a thioketyl radical.³³

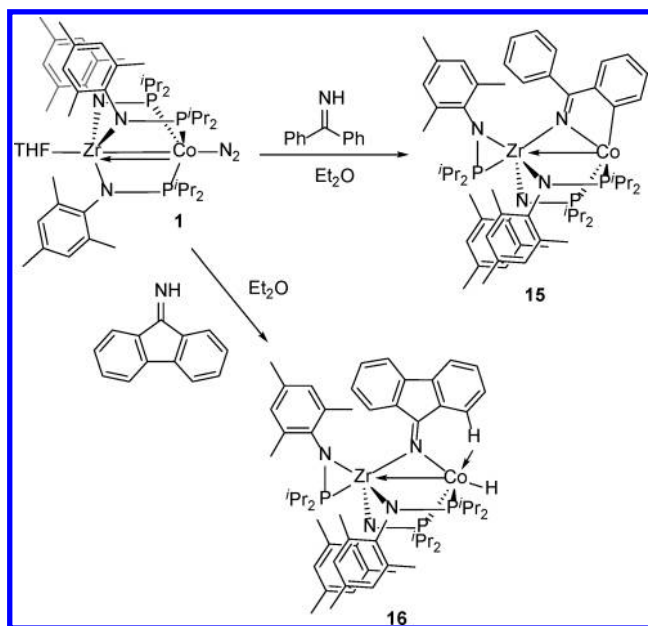
Although cleavage of a C=S bond is known to occur with Mo and W complexes, affording μ -sulfide carbene complexes,¹⁰ thermolysis of complex **12** did not result in C=S bond cleavage to form a carbene analogous to **3**. The thermal stability and connectivity of **12** contrast sharply with those of the benzophenone analogue and illustrate the importance of sequential one-electron-transfer reactions during the C=O bond cleavage reactions facilitated by **1**.

The inherent preference for the thiobenzophenone to react at the Co center can be overridden if the Co center has a strongly binding CO ligand in place of the more weakly bound N₂ ligand. Allowing thiobenzophenone to react with the reduced carbonyl complex **10** affords a new paramagnetic yellow complex (**13**) with a ^1H NMR spectrum similar to that of the isobenzopinacol coupling product **11** (Scheme 3). This result demonstrates that one-electron transfer to form a thioketyl radical complex is possible; however, without the carbonyl ligand present the preferred site of reactivity is at the cobalt rather than the zirconium side of the molecule.

To explore whether the η^2 -thiobenzophenone adduct **12** could be driven to isomerize to thioketyl-derived product **13** upon exposure to CO, a solution of complex **12** was exposed to an atmosphere of carbon monoxide. An immediate color change from purple to brown occurred, and the new diamagnetic complex **14** was formed rather than complex **13**. The ^1H NMR spectrum of **14** revealed different phosphinoamide ligand environments indicative of a structure in which one phosphinoamide ligand remains η^2 -bound to the Zr center, similar to the case for complex **12**. Further, the IR spectrum of complex **14** reveals a Co–CO stretch at 1904 cm^{-1} , which is substantially higher than that observed for **13** (1888 cm^{-1}). The solid-state structure of **14** confirms its connectivity as a CO adduct structurally similar to **12** (Figure 5). Notably, the Zr–Co bond length increases to 2.7072(5) Å in **14** upon binding of the π -acidic CO ligand. A similar elongation of the Co–Zr distance has been observed when comparing the coordinatively unsaturated (THF)Zr(MesNPⁱPr₂)₃Co complex with the CO- and N₂-bound derivatives **10** and **1**.^{23,34} The remainder of the geometrical parameters of **14** are largely similar to those of **12**, with the noticeable absence of an agostic interaction and a slight contraction of the C–S bond (1.787(3) Å) as the electron density at the Co center is diminished. Notably, thermolysis of complex **13** does not lead to the formation of **14**, and likewise, thermolysis of **14** does not lead to the formation of **13**.

Reactivity of 1 with Imines. Given the marked differences in reactivity between ketones and thioketones, we chose to expand our investigation to include the reactions between **1** and imines. In addition to a C=N bond polarized toward nitrogen, imines contain an N–H bond which may undergo activation upon exposure to the highly reduced Zr/Co complex. Allowing **1** to react with benzophenone imine afforded the dark green diamagnetic complex **15** (Scheme 4). Much like complex **12**, the ^1H NMR and $^{31}\text{P}\{^1\text{H}\}$ NMR spectra of **15** exhibited a 2:1 ratio of inequivalent ligand resonances, indicating an asymmetric structure with a phosphinoamide ligand η^2 -bound to the Zr center. The aryl rings of the benzophenone imine ligand were spectroscopically inequivalent and no N–H or Co–hydride signals were observed, suggesting that the benzophenone ligand may have undergone cyclometalation at Co.

Scheme 4



Support for the proposed connectivity of **15** was provided by a solid-state structure determined by X-ray crystallography, which revealed that cyclometalation of the aryl ring had indeed occurred (Figure 6). The C–N bond distance in **15** (1.315(6)

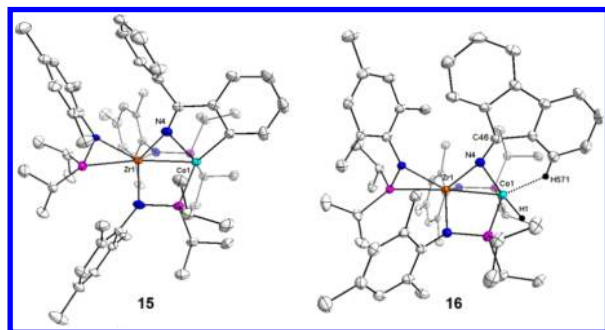


Figure 6. Displacement ellipsoid (50%) representation of complexes **15** and **16**. Hydrogen atoms have been omitted for clarity. Selected interatomic distances for **15** (Å): Zr1–Co1, 2.6166(9); Zr1–N4, 2.094(4); Co1–N4, 1.945(4); Co1–C48, 2.079(5); N4–C46, 1.315(6). Only one of the two crystallographically independent but structurally similar molecules in the asymmetric unit of complex **16** is shown. Selected interatomic distances for **16** (Å, with distances in second independent molecule in brackets): Zr1–Co1, 2.5087(5) [2.5217(5)]; Zr1–N4, 2.149(2) [2.123(2)]; Co1–N4, 1.901(2) [1.903(2)]; C46–N4, 1.306(4) [1.315(4)]; Co1–H571, 2.010 [2.059]; Co1–H1, 1.43 [1.38(4)].

Å) is between that of a single and double bond, in comparison to a zirconocene complex containing both a $[\text{Ph}_2\text{C}=\text{N}]^-$ ligand (C–N distance 1.257(5) Å) and a $[\text{Ph}_2\text{HC}=\text{NH}]^-$ ligand (C–N distance 1.372(6) Å),³⁵ and is similar to the C–N distances in a Ti/Co heterobimetallic complex featuring two bridging $[\text{N}=\text{CHPh}]^-$ ligands (1.31(2) and 1.30(2) Å).³⁶ The Zr–N and Co–N distances associated with the deprotonated imine functionality are similar (2.094(4) and 1.945(4) Å, respectively), suggesting a relatively symmetric bridging mode. The distance between the Co center and the bound aryl carbon atom (C48) is 2.079(5) Å, which is long relative to the typical range of Co–C_{aryl} bonds reported in the

literature (1.89–2.07 Å).³⁷ This elongation is likely the result of constraints imparted by the bridging nature of the imine anion.

The reaction pathway to form **15** likely involves activation of the imine N–H bond by Co to form a putative Co–H bond, followed by cyclometalation at the ortho position of one of the aryl rings and extrusion of H₂. The intermediacy of a Co–H during the formation of **15** is supported by the reaction between **1** and fluorenoneimine, which affords a red-purple diamagnetic complex **16** containing a Co–hydride observable by ¹H NMR spectroscopy at –14.03 ppm (Scheme 4). The spectroscopic features of **16** are largely similar to those of **15**, with the exception of the hydride resonance, suggesting a bridged structure resulting from activation of the imine N–H bond without cyclometalation. Cyclometalation also does not occur upon thermolysis of complex **16**, likely due to the decreased flexibility of the fused-ring system.

The structure of complex **16** was determined using single-crystal X-ray diffraction, confirming the proposed connectivity (Figure 6). The C–N bond in **16** is identical with that of **15**, with steric constraints imparting a less symmetrically bridged geometry with slightly elongated Zr–N distance (2.150(4) Å)³⁸ and contracted Co–N distance (1.901(3) Å) in comparison to that in complex **15**. In addition to a Co-bound hydride ligand, the coordination sphere of Co is completed by an agostic interaction from one of the ortho hydrogen atoms of the fluorenone ring with a Co–H distance of ~2.01 Å. This structural snapshot reveals a likely intermediate on the pathway for the ortho-metalation process that occurs with benzophenone imine.

From these results, it appears that activation of the N–H σ bond of the imine substrates is the preferred mode of reaction rather than the formation of ketimanyl radicals on the Zr side of the heterobimetallic complex. Allowing **1** to react with an imine substrate without an N–H bond, *N*-phenylfluorenone imine, in an attempt to induce C–N bond cleavage did not result in the formation of a new complex, and the unreacted starting materials were observed by ¹H NMR spectroscopy. The increased steric demand of *N*-phenylfluorenone imine may make displacement of THF and coordination unfavorable, and likewise the formation of a η^2 -bound imine structure similar to **12** may be sterically disfavored, resulting in no reaction with this substrate.

CONCLUSIONS

In summary, we have discovered that single-electron reduction of ketones by the reduced heterobimetallic complex (THF)-Zr(MesNP^{*i*}Pr₂)₃Co–N₂ (**1**) cleanly affords ketyl radical complexes either as transient intermediates en route to radical coupling products such as **4** or as observable species such as **5** and **7**. The electronic parameters of the diaryl ketones dictate the formation of a simple ketone adduct or a ketyl radical complex, with more electron donating aryl substituents disfavoring electron transfer. In contrast to the simple one-electron reduction observed for some C=O bonds, the reaction between **1** and C=S and C=N bonds does not afford thioketyl or ketimanyl radical products. Rather, thioketones coordinate through the π bond to the cobalt center (**12**). If, however, the Co side of the molecule is blocked by CO, the formation of a thioketyl radical dimer product can be observed (**13**). Addition of CO to complex **12** does not result in conversion to **13**, but instead a simple CO adduct **14** is observed. Finally, we discovered that imines undergo preferential N–H bond activation over one-electron reduction.

Activation of the N–H bond occurs to form a Co–H complex in the case of **16**, and this is a proposed intermediate on the pathway for the formation of cyclometalated benzophenoneimine complex **15**.

EXPERIMENTAL SECTION

General Considerations. All manipulations were carried out under an inert atmosphere using a nitrogen-filled glovebox or standard Schlenk techniques unless otherwise noted. All glassware was oven- or flame-dried immediately prior to use. Diethyl ether was obtained as HPLC grade without inhibitors; pentane and benzene were obtained as ACS reagent grade. All protio solvents were degassed by sparging with ultrahigh-purity argon and dried via passage through columns of drying agents using a Seca solvent purification system from Pure Process Technologies. Benzene-*d*₆ was degassed and dried over 4 Å molecular sieves before use. All ¹H NMR spectra were obtained at 400 MHz and recorded relative to residual protio solvent. Complexes **1–4** and **10** were synthesized according to literature procedures.^{16,17,23,34} All other reagents and solvents were obtained from commercial sources and used without further purification. Infrared spectra were recorded on a Varian 640-IR spectrometer controlled by Resolutions Pro software. UV–vis spectra were recorded on a Cary 50 UV–vis spectrophotometer using Cary WinUV software. Elemental microanalyses were performed by Complete Analysis Laboratories, Inc., Parsippany, NJ.

(C₁₃H₉)-O-Zr(MesNPⁱPr₂)₃Co-N₂ (5**).** In a 20 mL scintillation vial, (THF)Zr(MesNPⁱPr₂)₃CoN₂ (88 mg, 0.088 mmol) was dissolved in 2 mL of diethyl ether. To this solution was added a solution of fluorenone (19 mg, 0.11 mmol) in 2 mL of diethyl ether. After 5 min of swirling, the green solution was allowed to stand at –35 °C for 12 h. The greenish brown supernatant was decanted from the crystalline solid and discarded. The red-brown solid was washed once with cold pentane and then dried in vacuo to afford 76 mg (77%) of crystalline complex **5**. ¹H NMR (400 MHz, C₆D₆): δ 57.72 (s, 2H), 54.70 (s, 2H), 6.71 (s, 6H), 6.34 (s, 18H), 3.86 (s, 5H), 3.00 (s, 2H), 1.97 (s, 9H), –0.84 (s, 18H). UV–vis (C₆H₆; λ, nm (ε, M^{–1} cm^{–1})): 350 (8.0 × 10³), 365 (8.3 × 10³), 399 (3.9 × 10³), 505 (1.4 × 10³). Evans' method (298 K, C₆D₆): 2.46 μ_B. IR (C₆H₆): 2059 cm^{–1} (Co–N₂). Anal. Calcd for C₅₈H₈₃N₅OP₃CoZr: C, 62.79; H, 7.54; N, 6.31. Found: C, 62.70; H, 7.49; N, 6.25.

(C₁₃H₉)-O-Zr(MesNPⁱPr₂)₃Co-N₂ (6**).** In a 20 mL scintillation vial, complex **5** (32 mg, 0.029 mmol) was dissolved in 2 mL of cyclohexadiene. After the mixture was stirred at 25 °C for 16 h, the initial red color changed to yellow. The volatiles were removed in vacuo. The yellow residue was dissolved in diethyl ether and the solution filtered through a plug of Celite. The filtrate was concentrated to dryness in vacuo, affording 31 mg (99%) of **6** as a yellow powder. ¹H NMR (400 MHz, C₆D₆): δ 9.94 (s, 1H), 7.63–7.76 (m, 6H), 7.56 (s, 6H), 7.45 (m, 2H), 5.77 (s, 18H), 3.06 (br s, 6H), 2.64 (s, 18H), 2.15 (s, 9H), –1.59 (br s, 18H). UV–vis (C₆H₆; λ, nm (ε, M^{–1} cm^{–1})): 288 (6.4 × 10⁴), 311 (1.2 × 10⁴), 347 (6.0 × 10³). Evans' method (298 K, C₆D₆): 2.02 μ_B. IR (C₆H₆): 2044 cm^{–1} (Co–N₂). Anal. Calcd for C₅₈H₈₄N₅OP₃CoZr: C, 62.74; H, 7.63; N, 6.31; Found: C, 62.63; H, 7.74; N, 6.19.

(4-Me-C₆H₄)₂CO-Zr(MesNPⁱPr₂)₃Co-N₂ (7**).** In a 20 mL scintillation vial, (THF)Zr(MesNPⁱPr₂)₃CoN₂ (22 mg, 0.022 mmol) was dissolved in 0.5 mL of C₆D₆. To this solution was added a solution of (4-CH₃-C₆H₄)₂CO (4.6 mg, 0.022 mmol) in 1 mL of C₆D₆. After 30 s of swirling, the red solution was analyzed immediately due to the inherent instability of complex **7**. After prolonged standing, red complex **7** was transformed into yellow complex **8**. ¹H NMR (selected signals, spectrum is contaminated with the alkoxide generated by H atom abstraction from the THF present in the starting compound, 400 MHz, C₆D₆): δ 8.19 (s, 1H), 7.40 (s, 2H), 7.06 (s, 6H), 4.16 (br s, 12H), 2.74 (s, 18H), 2.34 (s, 9H), 2.18 (s, 6H), 0.21 (br s, 24H). IR (C₆H₆): 2045 cm^{–1} (Co–N₂). Due the instability of complex **7**, satisfactory elemental analysis data was not obtained.

(4-Me-C₆H₄)₂CHO-Zr(MesNPⁱPr₂)₃Co-N₂ (8**).** In a 20 mL scintillation vial, (THF)Zr(MesNPⁱPr₂)₃CoN₂ (103 mg, 0.102

mmol) was dissolved in 2 mL of THF. To this solution was added a solution of (4-Me-C₆H₄)₂CHO (22 mg, 0.10 mmol) in 2 mL of THF. After 5 min of swirling, the solvent was removed from the brown-yellow solution in vacuo. The residue was extracted into pentane and the extract filtered through a plug of Celite. The brown-yellow filtrate was concentrated to a final volume of 1 mL and then was allowed to stand at –35 °C for 12 h. The brownish supernatant was decanted from the crystalline solid and discarded. The yellow solid was then dried in vacuo to afford 47 mg (40%) of complex **8**. ¹H NMR (400 MHz, C₆D₆): δ 9.28 (s, 1H), 8.00 (d, *J* = 8.0 Hz, 4H), 7.53 (s, 6H), 7.15 (d, *J* = 8.0 Hz, 4H), 5.76 (s, 18H), 3.45 (br s, 6H), 2.72 (s, 18H), 2.33 (s, 6H), 2.17 (s, 9H), –1.71 (s, 18H). Evans' method (298 K, C₆D₆): 1.67 μ_B. UV–vis (C₆H₆; λ, nm (ε, M^{–1} cm^{–1})): 289 (1.6 × 10⁴), 358 (5.0 × 10³). IR (C₆H₆): 2043 cm^{–1} (Co–N₂). Satisfactory elemental analysis was collected on complex **8** without the labile N₂ ligand, which presumably dissociates prior to analysis. Anal. Calcd for C₆₀H₉₀N₃OP₃CoZr: C, 64.78; H, 8.15; N, 3.78. Found: C, 64.67; H, 8.18; N, 3.78.

(NMe₂-C₆H₄)₂CO-Zr(MesNPⁱPr₂)₃Co-N₂ (9**).** In a 20 mL scintillation vial, (THF)Zr(MesNPⁱPr₂)₃CoN₂ (67 mg, 0.067 mmol) was dissolved in 2 mL of tetrahydrofuran. To this solution was added a solution of (4-NMe₂-C₆H₄)₂CO (18 mg, 0.067 mmol) in 2 mL of tetrahydrofuran. After 5 min of swirling, the solvent was removed in vacuo from the brown-yellow solution. The residue was triturated with pentane to afford 66 mg (82%) of dark brown complex **9**. ¹H NMR (400 MHz, C₆D₆): δ 6.74 (s, 6H), 6.29 (br s, 4H), 3.15 (br s, 4H), 2.54 (s, 18H), 2.49 (s, 18H), 2.18 (s, 9H), 1.87 (br s, 18H), 1.62 (brm, 18H). ³¹P{¹H} NMR (162 MHz, C₆D₆): δ 50.3 (br s). ¹³C{¹H} NMR (100 MHz, THF-*d*₈): δ 153.37, 149.23, 134.78, 132.26, 131.08, 130.20, 129.18, 127.57, 111.09, 45.44, 39.99, 23.22, 23.15 (two signals overlapping), 20.38. UV–vis (C₆H₆; λ, nm (ε, M^{–1} cm^{–1})): 298 (3.2 × 10⁴), 347 (4.8 × 10⁴). IR (C₆H₆): 2044 cm^{–1} (Co–N₂), 1601 cm^{–1} (C=O). Repeated attempts to obtain satisfactory elemental analysis results were unsuccessful with this complex, likely the result of its instability.

[(Ph₂CO)Zr(MesNPⁱPr₂)₃Co(CO)]₂ (11**).** In a 20 mL scintillation vial, complex **11** (61 mg, 0.061 mmol) was dissolved in 2 mL of diethyl ether. To this solution was added a solution of benzophenone (13 mg, 0.071 mmol) in 2 mL of diethyl ether. After 5 min of swirling at room temperature, the yellow-orange solution was filtered through a plug of Celite and the filtrate was allowed to stand at –35 °C for 12 h. The brownish yellow supernatant was decanted from the yellow crystalline solid and discarded. The yellow solid was dried in vacuo, affording 28 mg (40%) of complex **11**. ¹H NMR (400 MHz, C₆D₆): δ 9.74 (s), 9.40 (s), 9.03 (s), 8.84 (s), 8.72 (s), 8.67 (s), 8.44 (s), 8.18 (s), 8.07 (s), 7.96 (s), 7.87 (s), 7.78 (s), 7.68–7.58 (m), 7.42 (s), 7.29 (s), 6.93 (d, *J* = 8.0 Hz), 6.53 (br s), 5.93 (d, *J* = 8.0 Hz), 5.39 (s), 5.24 (br s), 4.85 (s), 4.58 (s), 4.19 (s), 3.56 (d), 3.49 (s), 3.37 (d, *J* = 8.0 Hz), 3.07 (s), 2.40 (s), 2.22 (s), 2.14 (s), 1.91 (s), 1.80 (s), 0.61 (br s), 0.30 (br s), –0.09 (br s), –0.48 (br s), –1.10 (br s), –2.72 (br s), –3.15 (br s), –4.00 (br s), –4.80 (br s). UV–vis (C₆H₆; λ, nm (ε, M^{–1} cm^{–1})): 335 (3.4 × 10⁴). Evans method (298 K, C₆D₆): 2.28 μ_B. IR (PhMe): 1890 cm^{–1} (Co–CO). Anal. Calcd for C₁₁₈H₁₇₀N₆O₄P₆Co₂Zr₂: C, 63.76; H, 7.71; N, 3.78; Found: C, 63.75; H, 7.64; N, 3.81.

(^η2-MesNPⁱPr₂)Zr(MesNPⁱPr₂)₂Co(S=CPh₂) (12**).** In a 20 mL scintillation vial, (THF)Zr(MesNPⁱPr₂)₃CoN₂ (103 mg, 0.103 mmol) was dissolved in 2 mL of diethyl ether. To this solution was added a solution of thiobenzophenone (21 mg, 0.10 mmol) in 2 mL of diethyl ether. After 10 min of swirling, the initial burgundy color of the solution changed to dark purple-red. The ether was removed in vacuo, and the residue was extracted into pentane. The residue was then extracted into benzene, and the solution was filtered through a plug of Celite. The filtrate was then frozen, and the benzene was lyophilized in vacuo, affording 100 mg (88%) of complex **12**. X-ray-quality crystals were grown from a concentrated solution of **12** in pentane. ¹H NMR (400 MHz, C₆D₆): δ 7.43 (d, *J* = 8.0 Hz, 2H), 7.32 (d, *J* = 8.0 Hz, 2H), 7.09 (m, 2H), 7.03 (d, *J* = 8.0 Hz, 1H), 6.99 (br s, 2H), 6.92 (m, 2H), 6.87 (br s, 1H), 6.76 (br s, 1H), 6.71 (br s, 2H), 3.14 (d, *J* = 8.0 Hz, 1H), 2.98 (s, 3H), 2.96 (s, 3H), 2.75 (s, 3H), 2.61 (s, 3H), 2.36 (s,

1H), 2.18 (s, 6H), 2.14 (s, 3H), 2.11 (s, 3H), 1.78 (s, 3H), 1.66 (dd, $J = 20.0, 8.0$ Hz, 3H), 1.52 (m, 3H), 1.43 (dd, $J = 20.0, 8.0$ Hz, 3H), 1.34 (dd, $J = 20.0, 8.0$ Hz, 3H), 1.23 (m, 3H), 1.10 (m, 3H), 1.04–0.98 (m, 6H), 0.96–0.79 (m, 14H), 0.47 (dd, $J = 20.0, 8.0$ Hz, 3H). $^{31}\text{P}\{^1\text{H}\}$ NMR (162 MHz, C_6D_6): δ 49.54 (br s), 15.90 (s). $^{13}\text{C}\{^1\text{H}\}$ NMR (100 MHz, $\text{THF}-d_8$): δ 165.37 (d, $J = 2.0$ Hz), 153.29, 150.19, 148.10 (d, $J = 13.0$ Hz), 147.70 (d, $J = 14.0$ Hz), 146.62 (d, $J = 14.0$ Hz), 133.71 (d, $J = 3.0$ Hz), 133.61 (d, $J = 3.0$ Hz), 133.19 (d, $J = 3.0$ Hz), 132.76, 132.12 (d, $J = 3.0$ Hz), 130.96, 130.81 (d, $J = 2.0$ Hz), 130.37 (d, $J = 2.0$ Hz), 130.13 (d, $J = 2.0$ Hz), 128.15, 127.99 (d, $J = 13.0$ Hz), 127.78 (d, $J = 10.0$ Hz), 127.04, 126.52, 125.66, 125.53, 121.53, 39.48, 35.55 (d, $J = 4.0$ Hz), 34.91 (d, $J = 10.0$ Hz), 33.14 (d, $J = 10.0$ Hz), 33.13, 32.67 (d, $J = 16.0$ Hz), 32.36 (d, $J = 7.0$ Hz), 22.56 (dd, $J = 30.0, 4.0$ Hz), 22.33, 21.95, 21.77 (d, $J = 11.0$ Hz), 21.28, 21.18 (d, $J = 11.0$ Hz), 20.92, 20.74 (d, $J = 7.0$ Hz), 20.41, 20.40 (d, $J = 18.0$ Hz), 19.95 (dd, $J = 30.0, 8.0$ Hz), 19.48 (d, $J = 12.0$ Hz), 18.81, 18.64 (d, $J = 7.0$ Hz), 18.44 (d, $J = 9.0$ Hz), 17.90 (d, $J = 9.0$ Hz), 12.47. UV–vis (C_6H_6 ; λ , nm (ϵ , $\text{M}^{-1} \text{cm}^{-1}$): 350 (8.7×10^3), 500 (1.7×10^3). Anal. Calcd for $\text{C}_{58}\text{H}_{85}\text{N}_3\text{P}_3\text{S}\text{CoZr}$: C, 63.36; H, 7.79; N, 3.82. Found: C, 63.19; H, 7.84; N, 3.56.

[(Ph₂CS)Zr(MesNPⁱPr₂)₂Co(CO)] (13). Complex 13 was synthesized from a solution of (THF)Zr(MesNPⁱPr₂)₃CoCO (10) generated in situ using the following procedure. In a 100 mL resealable Schlenk tube containing a stir bar, (THF)Zr(MesNPⁱPr₂)₃CoN₂ (156 mg, 0.156 mmol) was dissolved in 40 mL of tetrahydrofuran. Approximately half of the volatiles were removed in vacuo, resulting in a color change from the red N₂-ligated species to the blue-green N₂-free species. The reaction vessel was resealed, frozen, and back-filled with excess CO(g). As the solution thawed and was stirred, it turned to a red-orange color characteristic of complex 10. The solution was stirred for 10 min before being refrozen and evacuated. After the reaction mixture was rethawed, volatiles were removed in vacuo. The residue was dissolved in pentane and filtered through a plug of Celite. To the red filtrate was added a blue solution of thiobenzophenone (32 mg, 0.16 mmol) in 2 mL of pentane. After 5 min of swirling at room temperature, the brown-yellow solution was allowed to stand at –35 °C for 24 h to complete crystallization. The dark brown supernatant was decanted from the yellow-orange crystalline solid and discarded. The solid was dried in vacuo, affording 72 mg (41%) of complex 13. ^1H NMR (400 MHz, C_6D_6): δ 9.36, 9.13, 8.34, 8.18, 8.07, 7.91, 6.91, 6.78, 6.56, 6.30, 5.40, 5.18, 4.42, 4.34, 3.81, 3.50, 3.17, 3.08, 3.00, 2.73, 2.49, 2.28, 2.13, 1.83, 1.70, 1.56, 0.28, –0.62, –1.91, –2.19, –2.74, –3.43, –4.94. Evans' method (298 K, $\text{THF}-d_8$): 1.70 μ_{B} . UV–vis (C_6H_6 ; λ , nm (ϵ , $\text{M}^{-1} \text{cm}^{-1}$): 315 (3.6×10^4), 418 (4.6×10^3). IR (C_6H_6): 1888 cm^{-1} (Co–CO). Anal. Calcd for $\text{C}_{118}\text{H}_{170}\text{N}_6\text{O}_2\text{P}_6\text{S}_2\text{Co}_2\text{Zr}_2$: C, 62.85; H, 7.60; N, 3.73. Found: C, 62.71; H, 7.65; N, 3.64.

(η^2 -MesNPⁱPr₂)Zr(MesNPⁱPr₂)₂Co(S=CPh₂)(CO) (14). In a 100 mL resealable Schlenk tube containing a stir bar, (THF)Zr(MesNPⁱPr₂)₃CoN₂ (72 mg, 0.072 mmol) was dissolved in 40 mL of diethyl ether. To this solution was added a solution of thiobenzophenone (16 mg, 0.078 mmol) in 2 mL of diethyl ether. After 10 min of swirling, the initial burgundy color of the solution changed to dark purple-red. Approximately half of the volatiles were removed in vacuo, and the flask was sealed and removed from the glovebox. The reaction vessel was then frozen in N₂(l) and back-filled with excess CO(g). As the solution thawed and was stirred, it turned brown. The solution was stirred for 20 min at room temperature before being refrozen and evacuated. After thawing, the reaction mixture was reintroduced to the glovebox, and the volatiles were removed in vacuo. The brown residue was dissolved in pentane, and the solution was filtered through a plug of Celite. The filtrate was concentrated to a final volume of about 2 mL of pentane and then allowed to stand at –35 °C for 16 h to complete crystallization. The light brown supernatant was decanted from the dark brown crystalline material, affording 39 mg (48%) of complex 14. ^1H NMR (400 MHz, $\text{THF}-d_8$): δ 7.47 (br s, 3H), 6.83 (s, 2H), 6.80 (br s, 2H), 6.75 (s, 2H), 6.64 (s, 3H), 2.65 (s, 6H), 2.55 (m, 3H), 2.29 (s, 2H), 2.20 (s, 4H), 2.13 (s, 7H), 1.48 (m, 7H), 1.32–1.21 (m, 14H), 1.12–1.05 (m, 3H), 1.00 (m, 8H), 0.87 (m, 13H), 0.67 (br s, 6H). $^{31}\text{P}\{^1\text{H}\}$ NMR (162

MHz, C_6D_6): δ 78.04 (br s), 54.85 (br s), 22.75 (s). $^{13}\text{C}\{^1\text{H}\}$ NMR (100 MHz, $\text{THF}-d_8$): δ 214.47, 155.80, 149.20 (d, $J = 13.0$ Hz), 134.79, 134.03, 133.12, 132.82, 130.29, 130.11, 129.90, 129.33, 129.06, 128.10, 124.67, 73.12 (t, $J = 9.0$ Hz), 35.13 (d, $J = 8.0$ Hz), 34.90, 34.31, 28.53 (d, $J = 18.0$ Hz), 23.32 (dd, $J = 32.0, 7.0$ Hz), 23.03, 22.46 (d, $J = 7.0$ Hz), 21.61, 20.47, 20.33, 18.92 (d, $J = 18.0$ Hz), 17.57 (d, $J = 8.0$ Hz), 15.51, 14.21. IR (C_6H_6): 1904 cm^{-1} (Co–CO). UV–vis (C_6H_6 ; λ , nm (ϵ , $\text{M}^{-1} \text{cm}^{-1}$): 329 (1.1×10^4), 418 (3.9×10^3). Anal. Calcd for $\text{C}_{59}\text{H}_{85}\text{N}_3\text{OP}_3\text{S}\text{CoZr}$: C, 62.85; H, 7.60; N, 3.73. Found: C, 62.71; H, 7.74; N, 3.80.

(η^2 -MesNPⁱPr₂)Zr(μ -N=C(C₁₂H₉))(MesNPⁱPr₂)₂Co (15). In a 20 mL scintillation vial, (THF)Zr(MesNPⁱPr₂)₃CoN₂ (79 mg, 0.079 mmol) was dissolved in 2 mL of diethyl ether. To this solution was added a solution of benzophenone imine (16 mg, 0.088 mmol) in 2 mL of diethyl ether. After 5 min of swirling, the blue-green solution was concentrated to dryness. The residue was then extracted into benzene, and the solution was filtered through a plug of Celite. The filtrate was then frozen, and the benzene was lyophilized in vacuo, affording 62 mg (72%) of complex 15. X-ray-quality crystals were grown from a concentrated solution of 15 in pentane. ^1H NMR (400 MHz, C_6D_6): δ 8.39 (br s, 1H), 7.92 (br s, 1H), 7.47 (br s, 1H), 7.28 (d, $J = 8.0$ Hz, 2H), 7.24 (m, 1H), 7.07 (m, 1H), 6.93 (m, 2H), 6.87 (s, 2H), 6.75 (s, 2H), 6.47 (s, 2H), 2.75 (s, 6H), 2.29 (s, 6H), 2.17 (s, 3H), 2.16 (s, 6H), 2.09 (s, 6H), 1.63 (m, 6H), 1.49 (m, 2H), 1.26 (m, 1H), 0.97 (m, 6H), 0.82–0.68 (m, 21H), 0.38 (m, 6H). $^{31}\text{P}\{^1\text{H}\}$ NMR (162 MHz, C_6D_6): δ 69.95 (br s), 22.35 (s). $^{13}\text{C}\{^1\text{H}\}$ NMR (100 MHz, $\text{THF}-d_8$): δ 171.62 (dt, $J = 3.0, 8.0$ Hz), 151.43, 150.07 (t, $J = 7.0$ Hz), 149.64 (d, $J = 11.0$ Hz), 143.44, 142.62 (d, $J = 10.0$ Hz), 135.44, 134.35 (d, $J = 24.0$ Hz), 133.22, 132.52 (d, $J = 23.0$ Hz), 131.29, 130.37, 130.17 (d, $J = 7.0$ Hz), 129.94 (d, $J = 15.0$ Hz), 129.59, 129.18, 128.71, 128.65 (d, $J = 3.0$ Hz), 128.34 (d, $J = 24.0$ Hz), 127.90, 127.69, 126.71, 126.05 (d, $J = 9.0$ Hz), 34.46 (d, $J = 7.0$ Hz), 32.43 (t, $J = 11.0$ Hz), 31.86, 28.67 (d, $J = 17.0$ Hz), 24.36, 23.32 (d, $J = 32.0$ Hz), 22.53, 21.82 (d, $J = 16.0$ Hz), 20.61 (d, $J = 14.0$ Hz), 20.44, 20.13, 19.08 (d, $J = 20.0$ Hz), 18.91, 18.40, 17.74 (d, $J = 10.0$ Hz). UV–vis (C_6H_6 ; λ , nm (ϵ , $\text{M}^{-1} \text{cm}^{-1}$): 288 (1.5×10^4), 344 (5.2×10^3). Anal. Calcd for $\text{C}_{58}\text{H}_{84}\text{N}_4\text{P}_3\text{CoZr}$: C, 64.48; H, 7.84; N, 5.19. Found: C, 64.50; H, 7.95; N, 5.11.

(η^2 -MesNPⁱPr₂)Zr(μ -N=C(C₁₂H₉))(MesNPⁱPr₂)₂Co(H) (16). In a 20 mL scintillation vial, (THF)Zr(MesNPⁱPr₂)₃CoN₂ (87 mg, 0.087 mmol) was dissolved in 2 mL of diethyl ether. To this solution was added a solution of fluorenone imine (16 mg, 0.089 mmol) in 2 mL of diethyl ether. After 10 min of swirling, the initially blue solution changed to dark purple. The ether was removed in vacuo, and the residue was extracted into pentane. The residue was then extracted into benzene, and the solution was filtered through a plug of Celite. The filtrate was then frozen, and the benzene was lyophilized in vacuo, affording 62 mg (72%) of complex 16. X-ray-quality crystals were grown from a concentrated solution of 16 in pentane. ^1H NMR (400 MHz, C_6D_6): δ 7.54 (d, $J = 8.0$ Hz, 1H), 7.49 (m, 2H), 7.36 (m, 1H), 7.22 (br m, 2H), 6.87 (s, 2H), 6.86 (s, 3H), 6.76 (s, 2H), 3.35 (d, $J = 8.0$ Hz, 1H), 2.66 (s, 6H), 2.43 (s, 6H), 2.32 (s, 6H), 2.29 (s, 3H), 2.15 (s, 6H), 1.64–1.58 (m, 8H), 0.96–0.91 (m, 7H), 0.29–0.84 (m, 13H), 0.74–0.68 (m, 14H), –14.03 (t, $J = 64$ Hz, 1H). $^{31}\text{P}\{^1\text{H}\}$ NMR (162 MHz, C_6D_6): δ 76.36 (br s), 24.34 (s). $^{13}\text{C}\{^1\text{H}\}$ NMR (100 MHz, $\text{THF}-d_8$): δ 166.85, 150.01 (d, $J = 10.0$ Hz), 149.56 (t, $J = 6.0$ Hz), 141.13, 140.62, 139.67, 134.38 (t, $J = 5.0$ Hz), 134.51, 134.16, 133.70 (d, $J = 2.0$ Hz), 132.38, 131.94, 130.50, 129.80, 128.86, 128.10, 126.32, 125.69, 125.10, 120.44 (d, $J = 21.0$ Hz), 119.30, 34.88, 34.46, 30.66 (d, $J = 13.0$ Hz), 30.46, 23.70 (d, $J = 4.0$ Hz), 23.16, 23.04, 22.61, 21.98, 21.42 (d, $J = 15.0$ Hz), 20.92 (t, $J = 6.0$ Hz), 20.69, 20.63, 20.49, 18.07 (d, $J = 14.0$ Hz), 14.23. UV–vis (C_6H_6 ; λ , nm (ϵ , $\text{M}^{-1} \text{cm}^{-1}$): 336 (4.5×10^3), 467 (2.0×10^3), 494 (1.9×10^3). Note: a Co–H stretching vibration was not observed by IR spectroscopy in solution (C_6H_6). Anal. Calcd for $\text{C}_{58}\text{H}_{84}\text{N}_4\text{P}_3\text{CoZr}$: C, 64.48; H, 7.84; N, 5.19. Found: C, 64.38; H, 7.76; N, 5.13.

X-ray Crystallography. All operations were performed on a Bruker-Nonius Kappa Apex2 diffractometer, using graphite-monochromated Mo $K\alpha$ radiation. All diffractometer manipulations, including data collection, integration, scaling, and absorption

corrections, were carried out using the Bruker Apex2 software.³⁹ Preliminary cell constants were obtained from 3 sets of 12 frames. Fully labeled diagrams and data collection and refinement details are included in Tables S1 and S2 and on pages S14–S27 of the Supporting Information.

Computational Details. All calculations were performed using Gaussian09, Revision A.02, for the Linux operating system.⁴⁰ Density functional theory calculations were carried out using a combination of Becke's 1988 gradient-corrected exchange functional⁴¹ and Perdew's 1986 electron correlation functional⁴² (BP86). A mixed-basis set was employed, using the LANL2TZ(f) triple- ζ basis set with effective core potentials for cobalt and zirconium,⁴³ Gaussian09's internal 6-311+G(d) set for heteroatoms (nitrogen, oxygen, and phosphorus), and Gaussian09's internal LANL2DZ basis set (equivalent to D95V⁴⁴) for carbon and hydrogen. Using crystallographically determined geometries as a starting point, the geometries were optimized to a minimum, followed by analytical frequency calculations to confirm that no imaginary frequencies were present.

■ ASSOCIATED CONTENT

■ Supporting Information

Text, figures, and tables giving experimental procedures, ¹H and ¹³C{¹H} NMR spectra of **5–9** and **11–16**, computational details, and X-ray crystallographic data collection and refinement details, CIF files giving crystallographic data, and a text file of all computed molecule Cartesian coordinates in a format for convenient visualization. This material is available free of charge via the Internet at <http://pubs.acs.org>.

■ AUTHOR INFORMATION

Corresponding Author

*E-mail for C.M.T.: thomasc@brandeis.edu.

Notes

The authors declare no competing financial interest.

■ ACKNOWLEDGMENTS

We acknowledge financial support from the U.S. Department of Energy under Award DE-SC0004019. C.M.T. is grateful for a 2011 Sloan Research Fellowship. Funding for S.L.M. was provided by the Camille and Henry Dreyfus Postdoctoral Program in Environmental Chemistry.

■ REFERENCES

- (1) Milstein, D.; Calabrese, J. C.; Williams, I. D. *J. Am. Chem. Soc.* **1986**, *108*, 6387–6389.
- (2) Blum, O.; Milstein, D. *J. Am. Chem. Soc.* **2002**, *124*, 11456–11467.
- (3) Li, Y.; Xie, Y.; Zhang, R.; Jin, K.; Wang, X.; Duan, C. *J. Org. Chem.* **2011**, *76*, 5444–5449.
- (4) Sevov, C. S.; Zhou, J.; Hartwig, J. F. *J. Am. Chem. Soc.* **2014**, *136*, 3200–3207.
- (5) Sage, V.; Burke, N. *Catal. Today* **2011**, *178*, 137–141.
- (6) McMurry, J. E.; Fleming, M. P.; Kees, K. L.; Krepski, L. R. *J. Org. Chem.* **1978**, *43*, 3255–3266.
- (7) Chisholm, M. H.; Foltling, K.; Klang, J. A. *Organometallics* **1990**, *9*, 602–606.
- (8) Bryan, J. C.; Mayer, J. M. *J. Am. Chem. Soc.* **1987**, *109*, 7213–7214.
- (9) Lutz, M.; Haukka, M.; Pakkanen, T. A.; Gade, L. H. *Organometallics* **2001**, *20*, 2631–2634.
- (10) Budzichowski, T. A.; Chisholm, M. H.; Foltling, K. *Chem. Eur. J.* **1996**, *2*, 110–117.
- (11) Ochiai, M.; Hashimoto, H.; Tobita, H. *Organometallics* **2012**, *31*, 527–530.
- (12) Fukumoto, K.; Sakai, A.; Oya, T.; Nakazawa, H. *Chem. Commun.* **2012**, *48*, 3809–3811.

(13) Krogman, J. P.; Foxman, B. M.; Thomas, C. M. *J. Am. Chem. Soc.* **2011**, *133*, 14582–14585.

(14) Napoline, J. W.; Bezpalko, M. W.; Foxman, B. M.; Thomas, C. M. *Chem. Commun.* **2013**, *49*, 4388–4390.

(15) Thomas, C. M.; Napoline, J. W.; Rowe, G. T.; Foxman, B. M. *Chem. Commun.* **2010**, *46*, 5790–5792.

(16) Marquard, S. L.; Bezpalko, M. W.; Foxman, B. M.; Thomas, C. M. *J. Am. Chem. Soc.* **2013**, *135*, 6018–6021.

(17) Zhou, W.; Marquard, S. L.; Bezpalko, M. W.; Foxman, B. M.; Thomas, C. M. *Organometallics* **2013**, *32*, 1766–1772.

(18) Covert, K. J.; Wolczanski, P. T.; Hill, S. A.; Krusic, P. J. *Inorg. Chem.* **1992**, *31*, 66–78.

(19) Covert, K. J.; Wolczanski, P. T. *Inorg. Chem.* **1989**, *28*, 4565–4567.

(20) Hou, Z.; Fujita, A.; Koizumi, T.-a.; Yamazaki, H.; Wakatsuki, Y. *Organometallics* **1999**, *18*, 1979–1985.

(21) Napoline, J. W.; Krogman, J. P.; Shi, R.; Kuppuswamy, S.; Bezpalko, M. W.; Foxman, B. M.; Thomas, C. M. *Eur. J. Inorg. Chem.* **2013**, 3874–3882.

(22) To test this hypothesis, a control reaction was conducted by the addition of 1 drop of *d*₈-THF to a benzene-*d*₆ solution of **7**, which resulted in immediate conversion to **8** with a substantially diminished ¹H NMR signal for the alkoxide at 9.28 ppm.

(23) Krogman, J. P.; Bezpalko, M. W.; Foxman, B. M.; Thomas, C. M. *Inorg. Chem.* **2013**, *52*, 3022–3031.

(24) Hansch, C.; Leo, A.; Taft, R. W. *Chem. Rev.* **1991**, *91*, 165–195.

(25) Loutfy, R. O.; Loutfy, R. O.; Taft, R. W. *Chem. Rev.* **1991**, *91*, 165–195.

(26) Rindorf, G.; Carlsen, L. *Acta Crystallogr., Sect. B* **1979**, *35*, 1179–1182.

(27) Weisheit, T.; Petzold, H.; Görls, H.; Mloston, G.; Weigand, W. *Eur. J. Inorg. Chem.* **2009**, *2009*, 3545–3551.

(28) Beck, R.; Sun, H.; Li, X.; Camadanli, S.; Klein, H.-F. *Eur. J. Inorg. Chem.* **2008**, *2008*, 3253–3257.

(29) Weigand, W.; Wunsch, R.; Robl, C.; Mloston, G.; Nöth, H.; Schmidt, M. Z. *Naturforsch., B* **2000**, *55*, 453–458.

(30) Pasquali, M.; Leoni, P.; Floriani, C.; Chiesi-Villa, A.; Guastini, C. *Inorg. Chem.* **1983**, *22*, 841–844.

(31) Beak, P.; Worley, J. W. *J. Am. Chem. Soc.* **1970**, *92*, 4142–4143.

(32) Beak, P.; Worley, J. W. *J. Am. Chem. Soc.* **1972**, *94*, 597–604.

(33) Alberti, A.; Benaglia, M.; Macciantelli, D.; Marcaccio, M.; Olmeda, A.; Pedulli, G. F.; Roffia, S. *J. Org. Chem.* **1997**, *62*, 6309–6315.

(34) Greenwood, B. P.; Rowe, G. T.; Chen, C.-H.; Foxman, B. M.; Thomas, C. M. *J. Am. Chem. Soc.* **2010**, *132*, 44–45.

(35) Lefeber, C.; Arndt, P.; Tillack, A.; Baumann, W.; Kempe, R.; Burlakov, V. V.; Rosenthal, U. *Organometallics* **1995**, *14*, 3090–3093.

(36) Zippel, T.; Arndt, P.; Ohff, A.; Spannenberg, A.; Kempe, R.; Rosenthal, U. *Organometallics* **1998**, *17*, 4429–4437.

(37) Based on a February 2014 search of the Cambridge structural database.

(38) For clarity, the distances in only one of the two crystallographically independent molecules in the asymmetric unit of **15** are discussed.

(39) *Apex 2, Version 2 User Manual, M86-E01078*; Bruker Analytical X-ray Systems, Madison, WI, 2006.

(40) Frisch, M. J.; Trucks, G. W.; Schlegel, H. B.; Scuseria, G. E.; Robb, M. A.; Cheeseman, J. R.; Scalmani, G.; Braone, V.; Mennucci, B.; Petersson, G. A., et al. *Gaussian09, Revision A.02*; Gaussian, Inc., Wallingford, CT, 2009. See the Supporting Information for the full reference.

(41) Becke, A. D. *Phys. Rev. A* **1988**, *38*, 3098–3100.

(42) Perdew, J. P. *Phys. Rev. B* **1986**, *33*, 8822–8824.

(43) Hay, P. J.; Wadt, W. R. *J. Chem. Phys.* **1985**, *82*, 299–310.

(44) Dunning, T. H.; Hay, P. J. In *Modern Theoretical Chemistry*; Schaefer, H. F., Ed.; Plenum: New York, 1976; pp 1–28.